Geochimica et Cosmochimica Acta 382 (2024) 91–102

Contents lists available at ScienceDirect

Geochimica et Cosmochimica Acta

journal homepage: www.elsevier.com/locate/gca

Controls on Li partitioning and isotopic fractionation in inorganic calcite

Oscar Branson [a,*,1], Joji Uchikawa [b,1], Madeleine S Bohlin [c,1], Sambuddha Misra [d,1]

[a] Department of Earth Sciences, University of Cambridge, Downing Street, Cambridge CB4 1BE, UK
[b] Department of Oceanography, University of Hawaii, 1000 Pope Rd., Honolulu, HI 96822, USA
[c] Department of Earth Sciences, Uppsala University, Villavägen 16, 752 36 Uppsala, Sweden
[d] Centre for Earth Sciences, Indian Institute of Science, Malleshwaram, Bengaluru 560012, Karnataka, India

ARTICLE INFO

Associate editor: Matthew S. Fantle

Keywords:
Calcite
Precipitation
Lithium
Partitioning
Fractionation
Isotope
Inorganic

ABSTRACT

The δ^7Li of marine carbonates has been interpreted as an archive of the evolution of seawater δ^7Li, and therefore continental weathering, through geological time. However, little is known about the incorporation of Li into calcium carbonate minerals and, consequently, the controls on Li partitioning (D_{Li}) and isotopic fractionation ($\Delta^7Li_{solid\text{-}fluid}$) associated with Li incorporation. Crucially, we lack a fundamental understanding of how Li partitioning and $\Delta^7Li_{solid\text{-}fluid}$ change in response to the chemical and physical conditions of crystal formation. Here, we present D_{Li} and $\Delta^7Li_{solid\text{-}fluid}$ data from a series of inorganic calcite precipitation experiments where temperature, and solution pH and dissolved inorganic carbon (DIC) were independently varied. We find D_{Li} values in the range 0.8–1.5 $\times$ 10^{-3}, which show no relationship with temperature, a strong positive correlation with pH, and a weak positive correlation with DIC. At face value, these patterns are inconsistent with the results of previous precipitation studies. However, the correlations with pH and DIC are consistent with a strong precipitation rate control on D_{Li} that aligns well with previous data, with a likely secondary influence from the incorporation of Li-HCO_3^0 ion pairs from solution. We find $\Delta^7Li_{solid\text{-}fluid}$ values in the range −6 to −2 ‰, which show no relationship with temperature or pH, and a weak positive correlation with DIC and crystal precipitation rate. These results do not agree with previously published data. Considered alongside previously published data, we observe no consistent relationship between $\Delta^7Li_{solid\text{-}fluid}$ and any reported physical or chemical experimental parameter, highlighting the need for substantial further work to determine whether systematic controls on Li isotopic fractionation exist in carbonate minerals, and whether they may be environmentally significant.

1. Introduction

There has been a growing interest in reconstructing past changes in isotopic composition of lithium (δ^7Li) in seawater as a tracer for continental silicate weathering (e.g., Pogge von Strandmann et al., 2013; Lechler et al., 2015), often using the calcite tests of foraminifera as a palaeoenvironmental archive (Hoefs and Sywall, 1997; Hall et al., 2005; Hathorne and James, 2006; Misra and Froelich, 2012). In all these studies, marine carbonate minerals are interpreted as a faithful archive of seawater δ^7Li. However, several recent studies have suggested that environmental variability may alter the incorporation of Li into foraminiferal calcite, and cause the δ^7Li of foraminifera to deviate from that of seawater. Studies of foraminifera from core-top samples have suggested that both seawater carbonate chemistry and temperature may exert a control on Li concentration in foraminifera (Lear et al., 2010; Lear and Rosenthal, 2015). Subsequent foraminifera culturing studies highlight a strong influence of carbonate chemistry on both the incorporation and isotopic fractionation of Li, although these studies disagree on whether these effects are caused by variability in DIC (Vigier et al., 2015) or pH (Roberts et al., 2018). These studies demonstrate that foraminiferal Li/Ca and δ^7Li are modified by environmental conditions, but it is difficult to discern the mechanism that drives this sensitivity because foraminifera are known to regulate the chemistry of their internal calcification fluid (Erez, 2003; de Nooijer et al., 2014), and changes in seawater temperature and carbonate chemistry tend to be highly correlated (Zeebe and Wolf-Gladrow, 2001). To understand whether these sensitivities are driven by biological mechanisms or the precipitation of the mineral itself, it is useful to examine the controls on Li incorporation in simpler inorganic precipitates.

Inorganic calcite precipitation experiments allow the detailed

* Corresponding author.
E-mail address: ob266@cam.ac.uk (O. Branson).
[1] Authors contributed equally to this work.

https://doi.org/10.1016/j.gca.2024.07.001
Received 15 July 2023; Accepted 1 July 2024
Available online 4 July 2024

investigation of the incorporation of non-constituent minor and trace elements into calcite and the isotopic fractionation associated with these incorporation processes. Since the pioneering works of Okumura & Kitano (1986) and Marriott et al. (2004a,2004b), an increasing number of inorganic experiments have focussed on the elemental and isotopic partitioning of Li during calcite precipitation from solutions (Füger et al., 2019, 2022; Day et al., 2021; Seyedali et al., 2021). As summarised recently in Chen et al. (2023), most of these studies hypothesise that calcite precipitation kinetics are a key modulator of Li elemental and isotopic partitioning in calcite (Füger et al., 2019, 2022; Day et al., 2021; Seyedali et al., 2021). However, it must be noted that the physico-chemical properties of the precipitating fluid (pH, DIC, temperature, *etc*.) all strongly influence precipitation kinetics but, in the published body of work, tend to be varied in tandem or with no systematic design. This makes it impossible to determine whether Li incorporation and isotopic fractionation depends on calcite precipitation kinetics or these highly correlated individual physico-chemical parameters. Furthermore, the formation of certain Li-bearing ion pairs such as Li-HCO_3^0 and Li-OH^0 in solutions have been proposed as potentially important for Li incorporation (Füger et al., 2019, 2022; Seyedali et al., 2021; Roberts et al., 2018). The formation of these ion pairs will be sensitive and highly specific to the types and concentrations of background electrolytes (and thus the overall ionic strength) in solution, and this idea requires careful testing across a wide range of electrolyte compositions to fully evaluate.

Here, we examine the effect of individually and systematically changing solution pH, DIC, and temperature on the paritioning and isotopic fractionation of Li on incorporation into inorganic calcite. We examine our data in context of previously published data, and consider the extent to which kinetic processes may explain the trends in these combined data.

2. Methods

2.1. Calcite precipitation

Inorganic calcite precipitation experiments were conducted at the University of Hawaii using a pH-stat system that has been extensively documented elsewhere (Sanyal et al., 2000; Zeebe and Sanyal, 2002; Uchikawa et al., 2015, 2017, 2023). Briefly, calcite is precipitated as an overgrowth onto calcite seeds in a 1.07 L temperature-controlled sealed reaction vessel with negligible headspace. The precipitation reaction is maintained at relatively constant chemical conditions using a titration system coupled to a pH electrode calibrated to NIST buffer solutions. The titrator was programmed to dose 0.3 M Na_2CO_3 solution upon 0.01 unit of pH decline caused by calcite precipitation to replenish alkalinity and DIC in 2:1 M ratio (Zeebe and Wolf-Gladrow, 2001). This kept the aqueous CO_2 chemistry relatively constant over the course of the experiments.

Calcite seeds used in these experiments were from the same batch as used in previous studies by Uchikawa et al. (2015,2017,2023). These seed crystals have been confirmed to be calcite by raman spectroscopy and X-ray diffraction analyses, and electron micrographs reveal that the seed crystals are rhombohedral with a typical long-axis length of ~10 μm. We employed the same method as Uchikawa et al. (2015,2017,2023) to calculate the fraction of newly grown material in our experiments using a $\delta^{13}C$ mass-balance approach. Seeds had a $\delta^{13}C_{seed}$ value of -17.87 ± 0.07 ‰ (VPDB, 1σ, $n = 5$), whereas the 0.3 M Na_2CO_3 solution used as the DIC-source for experimental solutions (see below) and as the titrant had a $\delta^{13}C_{solution}$ of approximately + 390 ‰. Batches of the Na_2CO_3 solution were prepared by dissolving a combination of unlabelled Na_2CO_3 and 99 % ^{13}C Na_2CO_3 (Cambridge Isotope Laboratories, CLM-306-1) into N_2-bubbled CO_2-free Milli-Q deionized H_2O (DIW). After each batch was prepared, 0.3 mmol of CO_3^{2-} from a 1 mL aliquot of the solution was quantitatively precipitated as $BaCO_3$ by reaction with 0.2 g of $BaCl_2{\cdot}2H_2O$ powder (8.2 mmol of Ba^{2+}) within a N_2-flushed glove-bag. Five replicate $BaCO_3$ precipitates were prepared for each ^{13}C-spiked solution, all of which produced at least 98 % of the theoretical or stoichiometrically-expected yield. As discussed elsewhere (Beck et al., 2005; Uchikawa and Zeebe, 2012; Uchikawa et al., 2021), these $BaCO_3$ precipitates quantitatively captured the $\delta^{13}C$ values of the DIC in the solution, and were measured to determine the $\delta^{13}C_{DIC}$ of each batch of the Na_2CO_3 solution. The $\delta^{13}C$ of newly-grown calcite overgrowths ($\delta^{13}C_{OG}$) precipitated from the solution (dominated by HCO_3^- in the pH range where our experiments were conducted) was then calculated using the ^{13}C fractionation factor between CO_3^{2-} and HCO_3^- derived in Zeebe and Wolf-Gladrow (2001) from the work of Zhang et al. (1995), and between HCO_3^- and calcite established by Romanek et al. (1992). These well-constrained $\delta^{13}C$ end-member values allow us to determine the proportion of the seeds and newly grown calcite in our precipitates (i.e. f_{OG} = overgrowth/total mass, see Uchikawa et al., 2015):

$$f_{OG} = \frac{{}^{13}A_{sample} - {}^{13}A_{seed}}{{}^{13}A_{OG} - {}^{13}A_{seed}} \quad (1)$$

where ^{13}A represents the fractional abundance of ^{13}C in the sample ($^{13}C/(^{12}C + {}^{13}C)$, ignoring ^{14}C). We use ^{13}A instead of $\delta^{13}C$ in these calculations to avoid non-linear mixing behaviour of isotope ratios when dealing with values that are far from zero (Zeebe and Wolf-Gladrow, 2001). These units are related to the more familiart $\delta^{13}C$ by:

$$\delta^{13}C = \left[\frac{\left(\frac{{}^{13}A}{1 - {}^{13}A} \right)}{R_{VPDB}} - 1 \right] \times 1000 \quad (2)$$

The quantity f_{OG} may also be calculated from the weights of the initial seeds and the final precipitate, but this is vulnerable to sample losses during filtration, and potential partial dissolution during the sample rinsing with DIW (see below). Our ^{13}C method bypasses these limitations to provide an accurate measure of newly grown material in each experiment. The strong ^{13}C spikes used in our experiment impose some analytical challenges for determining $\delta^{13}C_{BaCO3}$ and $\delta^{13}C_{sample}$ values because they are substantially higher than available carbonate standards. However, we note that the strength of these spikes is advantageous in minimising the error in the calculated f_{OG} values arising from uncertainties in $\delta^{13}C$ sample analyses, or in the fractionation factors used for calculating $\delta^{13}C_{OG}$. For example, introducing a ± 5 ‰ error in $\delta^{13}C_{OG}$ or $\delta^{13}C_{Sample}$ in Eq. 1 leads to only about 1.5 % error in the calculated f_{OG} value (compared to about 4.5 % if using a more moderate ^{13}C spike of + 100 ‰), as highlighted in Uchikawa et al. (2015,2017).

Note also that we applied a ^6Li-spike in our experimental solutions ($\delta^7Li_{Fluid-LSVEC} = -669 \pm 0.5$ ‰) to facilitate ^6Li magic angle spinning nuclear magnetic resonance analyses to investigate coordination of Li in the future. The spike (99.5 % ^6Li Li_2CO_3 dissolved in ultrapure HCl to a concentration of 1000 ppm) was applied to our stock solution of 0.1 M LiCl. The ^6Li-enriched Li_2CO_3 was purchased from Sigma Aldrich (MERCK® 99.5 % $^6Li_2CO_3$; CAS No. 25890-20-4).

Experimental solutions (1 L) were prepared by adding stock solutions of $CaCl_2$, ^6Li-spiked LiCl and ^{13}C-spiked Na_2CO_3 into the N_2-bubbled CO_2-free DIW adjusted to experimental temperatures. A small amount of HCl was also added to adjust solution pH to the target condition. The solution was transferred into the reaction vessel and first titrated with 0.3 M NaOH to desired pH values. After ~1.5 h of pH stabilisation (after which the solution is at chemical equilibrium), the titrant was switched to 0.3 M ^{13}C-spiked Na_2CO_3 solution and 40 mg of the calcite seeds were introduced into the reaction vessel. Note that our experimental solutions were saturated with respect to calcite in all cases, but not to the extent where precipitation would occur spontaneously (i.e., no homogeneous nucleation). Calcite precipitation began to occur only after addition of the seeds, which was discernible by steady decline in solution pH (see Fig. 3 in Uchikawa et al., 2015). Experiments were terminated after about 1 mL of the Na_2CO_3 titrant was dosed, corresponding to 22–25 mg of new calcite overgrowth. Calcite samples (seeds + overgrowth) were

subsequently collected by vacuum filtration, rigorously rinsed with DIW, dried at 65 °C overnight and stored in acid-cleaned vials until geochemical analyses. Experimental solutions prior to seed addition and after filtration were also sampled for analyses.

The control experimental condition was $[Ca^{2+}]_{Total}$ = 6.71 mM, $[Li^{+}]_{Total}$ = 0.322 mM, $[DIC]_{Total}$ = 2.1 mM at pH_{NBS} = 8.0 and T = 25 °C, at which the calcite saturation index ($SI_{Calcite} = \log_{10}(\{Ca^{2+}\}\{CO_3^{2-}\}/K_{SP})$ was calculated to be about 1.04 (n = 7, see Section 2.5). From this control condition we varied the solution pH, [DIC] and temperature individually to modify the degree of calcite saturation and thereby precipitation kinetics. At least triplicate runs were performed for each experimental condition. Prior to these experiments, we also conducted blank runs for which no LiCl solution was added to the experimental solutions (other experimental conditions were identical to the control). These blank runs resulted in calcite samples with negligible Li (Li/Ca < 1 μmol/mol), supporting the lack of contamination biases in our calcite precipitation experiments.

2.2. $\delta^{13}C$ analyses

Carbon (and oxygen) isotope analyses of our precipitates were performed at The Godwin Laboratory for Palaeoclimate Research at the University of Cambridge. Approximately 50–200 μg of dried homogenised sample was transferred to Exetainer vials and sealed with silicone rubber septa using a screw cap. The samples were flushed with CP grade helium and then acidified with 104 % orthophosphoric acid, left to react for 1 h at 70 °C, and then analysed using a Thermo Gasbench preparation system attached to a Thermo Delta V mass spectrometer in continuous flow mode. Each run of samples was accompanied by repeat analyses of 2 in-house standards (Carrara Z and Fletton Clay). Carrara Z has been calibrated to VPDB using the international standard NBS19. The results are reported with reference to the international standard VPDB and the precision is better than ± 0.08 ‰ for $\delta^{13}C$.

2.3. Li/Ca analyses

Analyses of Li/Ca and Li isotope ratios were conducted at the Department of Earth Sciences, University of Cambridge. All acids used were doubly distilled and diluted with 18.2 MOhm MilliQ DIW. Approximately 30 mg of carbonate sample was weighed into precleaned 0.5 mL microcentrifuge tubes. To remove excess salts and surface impurities, 0.4 mL MilliQ DIW was added and the vials were sonicated for 20 min. The samples were then centrifuged, and the supernatant was pipetted off and discarded. The procedure was repeated twice more using 0.001 N HCl. The samples were then dissolved in 0.3 mL of 1.5 N HCl.

Calcium concentrations of the calcite and fluid samples were determined by inductively coupled plasma optical emission spectroscopy (ICP-OES) on an Agilent 5100 using matrix matched calibration standards. These results were used to dilute the samples to a constant Ca concentration of 10 ppm and Li/Ca ratios were then determined by inductively coupled plasma mass spectrometry (ICP-MS) on a ThermoScientific ElementXR, following the procedure detailed in Misra et al. (2014). Each analytical session was calibrated using matrix matched multi-element calibration standards, and reproducibility was determined by repeated measurements of an in-house foraminifera standard solution (*Cam wuellerstorfi*) yielding a Li/Ca ratio of 15.9 ± 0.2 μmol/mol (2σ, n = 9), in good agreement with previously published values of 16.4 ± 0.8 (Misra et al., 2014). Samples were analysed in groups of 7 and bracketed by an in-house multi-element standard of identical [Ca] to correct for instrumental drift. Acid blanks were measured before and after each bracketing standard to monitor and correct for instrumental background.

2.4. Li purification and isotope analyses

The separation of Li from sample matrix elements followed the method of Bohlin et al. (2018). Adjustments were made to suit a smaller column volume of 1.5 mL to elute the Li fraction in 6 mL of dilute acid. This method uses high aspect ratio columns (20 cm height, 3.2 mm inner diameter) containing 1.5 mL AGMP-50 cation exchange resin. The resin was cleaned with 10 N HCl and MilliQ DIW between batches of samples and backwashed in MilliQ DIW prior to sample loading. Backwashing, or resuspension of the resin, allows the resin to resettle by gravity and provides a homogenous resin bed to improve sample loading. The resin was then conditioned with 5 ml 0.7 N HCl. Following which samples containing 1–2 ng Li were loaded in 150 μL of 0.7 N HCl. The columns were then washed with 4.5 mL 0.7 N HCl (pre-Li cut) and Li was eluted as a 6 mL cut. A 500 μL cut was collected before and after the Li cut to check for possible tailing of the Li peak to ensure a 100 % yield within the collected Li fraction. The samples were collected into acid cleaned Savillex® Teflon® vials and dried down on a hot plate at 80 °C overnight. Once dried, the samples were refluxed in ~ 500 μL of concentrated HNO_3 to break down possible organic matter originating from resin degradation. After ~ 24 h of refluxing, the samples were dried down and dissolved in 200 μL of 2 % HNO_3 (vol/vol) prior to isotope analysis.

Lithium isotope ratios were determined using a Thermo® Neptune® PLUS multi-collector inductively coupled plasma mass spectrometer (MC-ICP-MS) at the Department of Earth Sciences, University of Cambridge. Our analyses followed the standard sample bracketing (SSB) methodology as described in Bohlin et al. (2018). Purified Li samples were first concentration matched and then introduced using an APEX-IR sample introduction system with an ESI® 100 μL/min self-aspirating nebulizer. We used high sensitivity Ni Jet sampler and Ni X skimmer cones to achieve sensitivity of ~ 1 V per ppb. Two 10^{13} Ohm resistors on the L4 and H4 faraday cups were used for determination of ^{6}Li and ^{7}Li respectively. Samples were analysed at [Li] = ~0.4 ppb, yielding a current of 0.35–0.41 V on ^{7}Li. All samples were measured in duplicate and were bracketed by NIST SRM 8545 L-SVEC and acid blanks. Instrumental blanks were generally below 4 mV but reached a maximum of 10 mV, or < 2.5 % of sample signal intensity. All samples and standards were measured in blocks of 25 cycles with 8.4 s integration time. Each analytical session included determination of at least two of the instrumental control standards (Li^{6}-N and Li^{7}-N; Carignan et al., 2007). These secondary reference materials yielded values of −8.0 ± 0.6 ‰ (2σ, n = 16) and + 30.0 ± 0.4 ‰ (2σ, n = 7) respectively, which are analytically indistinguishable from published values (Carignan et al., 2007; Bohlin et al., 2018).

Established isotope standard(s) with extreme ^{6}Li enrichment that are isotopically similar to our ^{6}Li-spiked samples (~−670 ‰) are not available. Thus, NIST SRM 8545 L-SVEC was used for instrumental mass bias correction. This is not analytically ideal, as non-linearity in mass bias correction can be introduced with extreme enrichment/depletion from the composition of the bracketing standard. However, two factors help establish the accuracy of the isotopic data reported here. First, earlier work on more enriched ^{6}Li samples ($\delta^{7}Li$ ~ −960 ‰), which were analysed following identical analytical approach and determined on the same instrument, reported that the E13 amplifiers of the the Neptune® PLUS used for our analyses have a linear response between ion loading and beam size in the 0.015 to 0.450 V range (Llyod et al., 2018; Gout et al., 2019, 2021). This allows us to confidently apply the SSB strategy to these samples, which linearly interpolates the mass bias between bracketing standards to account for instrumental mass bias during isotope ratio determination. Second, if the mass bias of the instrument were variable and deviated from this linear assumption, we would expect to observe substantial variance between the same sample measured across different analytical sessions. To test this, multiple aliquots of two batches of ^{6}Li-enriched initial experimental fluids were separately column processed and measured during separate instrument

Table 1
Precipitation conditions, measurements of fluids and precipitates, and calculated overgrowth compositions in our study. All Li/Ca values are in mol/mol, and Δ^7Li is in ‰. All uncertainties are 1σ from repeat measurements.

		Solution					Precipitate			Overgrowth					
	Run #	Temp ℃	pH NBS	Li/Ca start $\times10^2$	Li/Ca end $\times10^2$	$\alpha^7Li_{L\text{-}SVEC}$	$\delta^{13}C_{PDB}$	Li/Ca $\times10^5$	$\alpha^7Li_{L\text{-}SVEC}$	f_{og}	$\log_{10}R$ mol/m^2/s	Li/Ca $\times10^5$	D_{Li} $\times10^3$	$\alpha^7Li_{L\text{-}SVEC}$	Δ^7Li
pH 7.8	1.1	25	7.80 ± 0.02	3.91 ± 0.12	3.85	0.33045 ± 0.00004	143.12	1.39 ± 0.04	0.33940 ± 0.00008	0.393 ± 0.002	−6.262 ± 0.005	3.41 ± 0.11	0.89 ± 0.04	0.3302 ± 0.0010	−0.6 ± 3.0
	1.2b				4.06		133.88	1.38 ± 0.04	0.33960 ± 0.00005	0.370 ± 0.002	−6.293 ± 0.005	3.59 ± 0.11	0.93 ± 0.04	0.3300 ± 0.0010	−1.2 ± 3.2
	1.3				3.94		128.44	1.41 ± 0.04	0.33868 ± 0.00013	0.357 ± 0.002	−6.338 ± 0.005	3.80 ± 0.12	0.99 ± 0.04	0.3291 ± 0.0010	−4.3 ± 3.3
pH 8.2	2.1	25	8.20 ± 0.02	3.63 ± 0.11	3.65	0.33052 ± 0.00003	145.89	2.19 ± 0.07	0.33544 ± 0.00008	0.400 ± 0.002	−5.636 ± 0.005	5.36 ± 0.17	1.47 ± 0.06	0.3297 ± 0.0006	−2.3 ± 1.9
	2.2				3.55		148.51	2.19 ± 0.07	0.33566 ± 0.00008	0.406 ± 0.002	−5.624 ± 0.006	5.28 ± 0.16	1.45 ± 0.06	0.3300 ± 0.0006	−1.9 ± 1.9
	2.3				3.49		151.74	2.15 ± 0.06	0.33495 ± 0.00013	0.414 ± 0.002	−5.611 ± 0.006	5.08 ± 0.16	1.39 ± 0.06	0.3293 ± 0.0006	−3.4 ± 2.1
pH 8.4	3.1	25	8.41 ± 0.02	3.92 ± 0.12	3.92	0.33051 ± 0.00003	153.10	2.41 ± 0.07	0.33533 ± 0.00007	0.417 ± 0.002	−5.402 ± 0.006	5.67 ± 0.18	1.44 ± 0.06	0.3303 ± 0.0005	−0.6 ± 1.7
	3.2				3.96		145.36	2.38 ± 0.07	0.33427 ± 0.00017	0.398 ± 0.002	−5.433 ± 0.005	5.86 ± 0.18	1.49 ± 0.06	0.3290 ± 0.0006	−3.8 ± 1.7
	3.3				4.01		153.00	2.33 ± 0.07	0.33439 ± 0.00010	0.417 ± 0.002	−5.432 ± 0.006	5.47 ± 0.17	1.39 ± 0.06	0.3292 ± 0.0006	−4.3 ± 2.0
0.5 x [DIC]	4.1	25	8.00 ± 0.04	3.56 ± 0.11	3.58	0.33055 ± 0.00004	128.17	0.13 ± 0.03	0.34082 ± 0.00006	0.356 ± 0.002	−6.471 ± 0.005	3.03 ± 0.10	0.85 ± 0.04	0.3288 ± 0.0013	−5.0 ± 4.0
	4.1b				3.58		128.17	0.13 ± 0.03	0.34100 ± 0.00006	0.356 ± 0.002	−6.471 ± 0.005	3.03 ± 0.10	0.85 ± 0.04	0.3290 ± 0.0013	−5.0 ± 4.0
	4.2				3.65		156.03	1.54 ± 0.05	0.33562 ± 0.00015	0.424 ± 0.002	−6.412 ± 0.006	3.52 ± 0.11	0.98 ± 0.04	0.3278 ± 0.0009	−8.1 ± 2.6
	4.3				3.67		159.75	1.04 ± 0.04	0.33624 ± 0.00008	0.433 ± 0.002	−6.383 ± 0.006	3.13 ± 0.10	0.87 ± 0.04	0.3278 ± 0.0009	−8.4 ± 3.1
	4.4				3.75		150.26	1.32 ± 0.04	0.33866 ± 0.00021	0.410 ± 0.002	−6.434 ± 0.006	3.10 ± 0.10	0.87 ± 0.04	0.3293 ± 0.0010	−5.0 ± 4.0
1.5 x [DIC]	5.1	25	8.00 ± 0.02	4.22 ± 0.13	4.32	0.33073 ± 0.00017	144.10	2.15 ± 0.06	0.33625 ± 0.00006	0.395 ± 0.002	−5.676 ± 0.005	5.32 ± 0.17	1.23 ± 0.05	0.3304 ± 0.0006	−0.7 ± 1.9
	5.2				4.12		145.79	2.12 ± 0.06	0.33569 ± 0.00014	0.399 ± 0.002	−5.683 ± 0.005	5.19 ± 0.16	1.20 ± 0.05	0.3298 ± 0.0007	−2.9 ± 1.9
	5.3				4.26		147.07	2.13 ± 0.06	0.33521 ± 0.00009	0.402 ± 0.002	−5.690 ± 0.005	5.17 ± 0.16	1.20 ± 0.05	0.3294 ± 0.0006	−4.5 ± 2.7
	5.4				4.61		151.49	2.18 ± 0.07	0.33535 ± 0.00020	0.413 ± 0.002	−5.681 ± 0.006	5.16 ± 0.16	1.20 ± 0.05	0.3298 ± 0.0006	−2.7 ± 2.5
	5.4				4.61		149.47	2.18 ± 0.07	0.33535 ± 0.00020	0.408 ± 0.002	−5.688 ± 0.006	5.22 ± 0.16	1.21 ± 0.05	0.3297 ± 0.0006	−2.8 ± 2.6
2 x [DIC]	6.1	25	8.00 ± 0.01	4.54 ± 0.14	4.61	0.33021 ± 0.00034	131.29	2.02 ± 0.06	0.33667 ± 0.00010	0.364 ± 0.002	−5.609 ± 0.005	5.41 ± 0.17	1.17 ± 0.05	0.3301 ± 0.0007	−0.4 ± 2.2
	6.2				4.57		146.49	2.29 ± 0.07	0.33449 ± 0.00014	0.401 ± 0.002	−5.544 ± 0.005	5.59 ± 0.17	1.21 ± 0.05	0.3291 ± 0.0006	−4.1 ± 1.9
	6.3				3.36		144.87	1.79 ± 0.05	0.33610 ± 0.00012	0.397 ± 0.002	−5.535 ± 0.005	4.39 ± 0.14	0.95 ± 0.04	0.3291 ± 0.0008	−4.1 ± 2.8
T = 35 °C	7.1	35	8.00 ± 0.02	3.79 ± 0.11	3.90	0.33170 ± 0.00040	147.19	1.81 ± 0.05	0.33735 ± 0.00016	0.404 ± 0.002	−5.666 ± 0.006	4.37 ± 0.14	1.12 ± 0.05	0.3305 ± 0.0008	−2.5 ± 2.3

(*continued on next page*)

Table 1 (*continued*)

		Solution					Precipitate			Overgrowth					
	Run #	Temp ℃	pH NBS	Li/Ca start $\times10^2$	Li/Ca end $\times10^2$	$\alpha^7Li_{L\text{-}SVEC}$	$\delta^{13}C_{PDB}$	Li/Ca $\times10^5$	$\alpha^7Li_{L\text{-}SVEC}$	f_{og}	$\log_{10}R$ mol/m^2/s	Li/Ca $\times10^5$	D_{Li} $\times10^3$	$\alpha^7Li_{L\text{-}SVEC}$	Δ^7Li
	7.2				3.85		131.59	1.74 ± 0.05	0.33722 ± 0.00015	0.365 ± 0.002	−5.717 ± 0.006	4.62 ± 0.15	1.18 ± 0.05	0.3296 ± 0.0008	−5.3 ± 2.5
	7.3				3.89		142.47	1.77 ± 0.05	0.33726 ± 0.00012	0.392 ± 0.002	−5.675 ± 0.006	4.39 ± 0.14	1.13 ± 0.05	0.3301 ± 0.0008	−3.4 ± 2.5
	7.3				3.89		141.80	1.77 ± 0.05	0.33726 ± 0.00012	0.390 ± 0.002	−5.678 ± 0.006	4.41 ± 0.14	1.13 ± 0.05	0.3301 ± 0.0008	−3.4 ± 2.5
T = 15 °C	8.1	15	8.00 ± 0.03	3.66 ± 0.11	3.90	0.33206 ± 0.00016	149.61	1.78 ± 0.05	0.33844 ± 0.00024	0.408 ± 0.002	−6.291 ± 0.005	4.25 ± 0.13	1.09 ± 0.05	0.3315 ± 0.0008	−1.5 ± 3.3
	8.2				3.80		152.34	1.93 ± 0.06	0.33755 ± 0.00026	0.414 ± 0.002	−6.298 ± 0.005	4.54 ± 0.14	1.16 ± 0.05	0.3312 ± 0.0007	−5.2 ± 2.7
	8.3a				3.92		147.34	1.93 ± 0.06	0.33737 ± 0.00023	0.402 ± 0.002	−6.322 ± 0.005	4.68 ± 0.15	1.20 ± 0.05	0.3309 ± 0.0007	−3.4 ± 2.8
	8.3b				3.92		147.34	1.93 ± 0.06	0.33792 ± 0.00014	0.402 ± 0.002	−6.322 ± 0.005	4.68 ± 0.15	1.20 ± 0.05	0.3315 ± 0.0007	−3.3 ± 2.9
Control1	C1.1	25	8.00 ± 0.02	4.03 ± 0.12	3.96	0.33036 ± 0.00004	145.01	1.89 ± 0.06	0.33529 ± 0.00005	0.397 ± 0.002	−5.925 ± 0.005	4.63 ± 0.15	1.17 ± 0.05	0.3287 ± 0.0007	−5.2 ± 2.2
	C1.2				3.60		146.12	1.83 ± 0.05	0.33642 ± 0.00009	0.400 ± 0.002	−5.910 ± 0.005	4.45 ± 0.14	1.13 ± 0.05	0.3296 ± 0.0007	−2.7 ± 2.3
	C1.3				3.04		142.75	1.62 ± 0.05	0.33774 ± 0.00013	0.392 ± 0.002	−5.928 ± 0.005	4.01 ± 0.13	1.01 ± 0.04	0.3299 ± 0.0009	−0.9 ± 3.5
	C1.4				4.00		140.72	1.83 ± 0.05	0.33587 ± 0.00017	0.387 ± 0.002	−5.946 ± 0.005	4.60 ± 0.14	1.16 ± 0.05	0.3289 ± 0.0008	−4.0 ± 2.6
Control2	C2.1	25	8.00 ± 0.02	3.83 ± 0.11	3.91	0.33158 ± 0.00004	132.01	1.81 ± 0.05	0.33624 ± 0.00006	0.366 ± 0.002	−5.983 ± 0.005	4.81 ± 0.15	1.23 ± 0.05	0.3289 ± 0.0008	−8.0 ± 2.4
	C2.2				4.64		136.13	1.90 ± 0.06	0.33666 ± 0.00022	0.376 ± 0.002	−5.968 ± 0.005	4.92 ± 0.15	1.26 ± 0.05	0.3298 ± 0.0008	−7.0 ± 2.2
	C2.3				4.06		127.91	1.69 ± 0.05	0.33844 ± 0.00020	0.356 ± 0.002	−5.978 ± 0.005	4.61 ± 0.15	1.18 ± 0.05	0.3305 ± 0.0009	−3.6 ± 2.6
	C2.3b				4.06		127.91	1.69 ± 0.05	0.33822 ± 0.00023	0.356 ± 0.002	−5.978 ± 0.005	4.61 ± 0.15	1.18 ± 0.05	0.3302 ± 0.0009	−2.7 ± 2.6

sessions. The ^{6}Li enriched fluids of batch 1 (used for the pH and DIC experiments) had a reproducibility of ± 0.3 ‰ (δ^7Li: −669.6 ± 0.3 ‰; 2σ; n = 7), and batch 2 (used for the temperature experiments) had a reproducibility of ± 1 ‰ (δ^7Li: −668.4 ± 1.0 ‰; 2σ; n = 5). Furthermore, procedural duplicates of three samples (Sample# 8.3, 4.1 and C2.3; see Table 1) yielded analytically indistinguishable δ^7Li values for each pair of measurements across different analytical sessions. The average δ^7Li of samples 8.3, 4.1 and C2.3 were −662.7 ± 0.2 ‰, −661.8 ± 0.1 ‰ and −659.4 ± 0.3 ‰ respectively (2σ, n = 2). Together, this confirms that our method produces accurate and precise results for heavily spiked samples across multiple analytical sessions. Finally, we note that isotopic data are interpreted as the difference between precipitate and solution (Δ^7Li: see Section 2.5 below). The observed variation in Δ^7Li space is ≤ 6 ‰, implying that any possible non-linearity in mass bias correction would lead to analytically unresolvable differences in the measured Δ^7Li.

2.5. Data processing and reporting

All raw data, along with code used to analyse the data and produce the graphs in this paper are available online (https://doi.org/10.5281/zenodo.11403415). Data processing, analysis and plotting was conducted in Python (version 3.11), making extensive use of the numpy (Harris et al., 2020), scipy (Virtanen et al., 2020), matplotlib (Hunter, 2007) and pandas (The pandas development team, 2023) libraries. Linear relationships in data were evaluated using a Wald Test, which tests the null hypothesis that the slope of a line is zero.

The fractional abundance of the final precipitate that grew in the experimental condition (f_{OG}) was calculated using a ^{13}C mass balance (Eq. (1)). This value was applied to unmix the Li/Ca and δ^7Li of the overgrowth and the seed crystal from measurements of Li/Ca in the precipitate and the seed crystals (0.8 ± 0.08 μmol/mol, 1σ, n = 2):

$$(Li/Ca)_{OG} = \frac{(Li/Ca)_{sample} - (1 - f_{OG})(Li/Ca)_{seed}}{f_{OG}} \quad (3)$$

and

$${}^7A_{OG} = \frac{{}^7A^{Li}_{meas}A_{meas} - {}^7A^{Li}_{seed}A_{seed}(1 - f_{OG})}{{}^{Li}A_{OG}f_{OG}} \quad (4)$$

where ^{7}A is the abundance of ^{7}Li in the material (^{7}Li/(^{7}Li + ^{6}Li)), and ^{Li}A is the fractional abundance of Li in the solid (^{Li}A = Li/Ca/(1 + Li/Ca)). Note that the δ^7Li of the seed crystals could not be determined due to their extremely low Li content, so was assumed to be identical to the L-

SVEC standard. Given the fraction of seed calcite, the ^{6}Li enriched composition of the overgrowth, and the order of magnitude Li concentration difference between the overgrowth and the seed, the choice of initial isotopic composition of the seed does not have a significant effect on subsequent calculations.

The distribution coefficient of Li into calcite is expressed as:

$$D_{\mathrm{Li}} = \frac{(\mathrm{Li}/\mathrm{Ca})_{solid}}{[\mathrm{Li}]/[\mathrm{Ca}]_{fluid}} \quad (5)$$

where $[\mathrm{Li}/\mathrm{Ca}]_{\mathrm{fluid}}$ for the calculation of D_{Li} is based on molar concentrations. The Li isotopic fractionation between calcite overgrowths and experimental solutions are expressed as:

$$\Delta^{7}\mathrm{Li}_{solid-fluid} = \delta^{7}\mathrm{Li}_{solid} - \delta^{7}\mathrm{Li}_{fluid} \quad (6)$$

Also note that the precipitating fluids, and hence the calcite overgrowths, were significantly enriched in ^{6}Li ($\delta^{7}\mathrm{Li}_{\mathrm{fluid\text{-}LSVEC}} \sim -670$ ‰; Table 1). This large difference in isotopic composition between L-SVEC and analyte (carbonate and precipitating fluid) precludes the useful consideration of the isotopic composition of our samples relative to L-SVEC, so we only consider the isotopic difference between the solid and the solution they were grown from.

Overgrowth precipitation rate in mol m^{-2} s^{-1} was calculated from the start volume of the seeds and the final volume of the precipitate by assuming that the newly grown material identified by the ^{13}C mass balance accreted to the seeds following a cubic growth geometry, such that:

$$R = \frac{\left(V^{1/3} - V_0^{1/3}\right)\rho_{calcite}}{2\,t\,M_{CaCO3}} \quad (7)$$

where V and V_0 are the volumes of the final precipitate and seed crystals in m^3, t is the experiment time in seconds, ρ is the density of calcite, M_{CaCO3} is the molecular weight of calcite, and R is precipitation rate in mol m^{-2} s^{-1}.

Solution speciation was calculated using PHREEQC (Parkhurst and Appelo, 1999) using the 'pitzer.dat' parameter database. The same method was also applied to re-calculate speciation data from previous studies to ensure that solution values are directly comparable between experiments.

3. Results

A summary of precipitation conditions, solution and precipitate measurements, and calculated overgrowth compositions can be found in Table 1.

3.1. Contribution of seed crystals and blank solutions

Calcite seeds had a Li/Ca of 0.8 ± 0.08 μmol/mol (1σ, $n = 2$), and calcite samples precipitated from blank runs in which no LiCl was added to the experimental solutions had Li/Ca of 0.95 ± 0.21 μmol/mol (1σ, $n = 4$). This is at least an order of magnitude lower than experimental samples (11–24 μmol/mol Li/Ca), indicating that the majority (>95 %) of Li present in our precipitates was incorporated during growth in our experimental solutions. This indicates that we have minimal Li contamination in our experimental systems, solutions, and calcite seeds.

3.2. Titration records of calcite precipitation

Titration plots for blank and control experiments were indistinguishable within analytical uncertainty (Fig. S1), indicating that these experiments proceeded at a nearly identical pace. Note that the only difference between the blank and control solutions was the addition of 0.322 mM LiCl to the control experimental solutions, demonstrating that the presence of LiCl used in our experiments has negligible impact on calcite precipitation kinetics. In other experimental solutions, the rate of titrant addition increased progressively with elevating solution pH, [DIC], and temperature. In all of our calcite precipitation experiments, the rate of titrant addition remained relatively consistent from the point of seed addition to the end of the experiment (Fig. S2-S4), indicating that precipitation proceeded at a consistent rate throughout each individual experiment. The three to five replicates conducted at each of our experimental conditions produced consistent titration curves within an experimental condition (compiled in Figures S2, S3, and S4 for pH, [DIC], and temperature experiments, respectively).

3.3. Excluded data

Two data points are excluded from the following data analysis: Sample 1.2 from the pH 7.8 experiment had an anomalously high (+7‰) $\Delta^{7}\mathrm{Li}_{\mathrm{solid\text{-}fluid}}$, and reanalysis (datum 1.2b) revealed a value more consistent with other precipitates grown in that condition; the initial isotope value for sample 1.2 was therefore excluded from analysis in favour of 1.2b. Sample 6.4 from the 2xDIC experiment had anomalously low δ^{13}C and δ^{18}O values compared to the entire sample set, alongside high D_{Li}; all data from this sample were excluded from analysis.

3.4. Overgrowth composition

Neither the partitioning of Li into the calcite overgrowth (D_{Li}), nor the isotopic fractionation of Li between solution and solid ($\Delta^{7}\mathrm{Li}_{\mathrm{solid\text{-}fluid}}$) showed any significant change between 15 and 35 °C ($p = 0.53$, Fig. 1A, and $p = 0.84$, Fig. 1E, respectively). We observe a strong increase in overgrowth D_{Li} with solution pH ($p < 0.01$, $R^2 = 0.86$), increasing from 0.95 to 1.5 across a pH range of 7.8 to 8.4 (Fig. 1B) but find no significant relationship between $\Delta^{7}\mathrm{Li}_{\mathrm{solid\text{-}fluid}}$ and pH ($p = 0.70$, Fig. 1F). We observe a significant increase in D_{Li} with solution DIC ($p < 0.01$, $R^2 = 0.49$), which increases from 0.95 to 1.2 between a DIC of 1000 and 3000 μmol/kg (Fig. 1C), with a slight decrease above 3000 μmol/kg. We find a weak positive relationship between $\Delta^{7}\mathrm{Li}_{\mathrm{solid\text{-}fluid}}$ and DIC ($p < 0.01$, $R^2 = 0.36$), which increases from −6 ‰ to −2.5 ‰ across the DIC range examined in our experiments (Fig. 1G).

Considered as a function of precipitation rate, we observe distinct patterns in the pH and DIC experiments compared to the temperature experiment (Fig. 1D & H). The pH and DIC experiments together show significant positive correlations between D_{Li} and precipitation rate (Fig. 1D, $p < 0.01$, $R^2 = 0.69$), and a weaker significant positive relationship between $\Delta^{7}\mathrm{Li}_{\mathrm{solid\text{-}fluid}}$ and precipitation rate (Fig. 1H, $p = 0.02$, $R^2 = 0.17$). The temperature experiments diverge substantially from these trends, exhibiting either no correlation or a weak negative relationship between precipitation rate and both D_{Li} (Fig. 1D, dashed line) and $\Delta^{7}\mathrm{Li}_{\mathrm{solid\text{-}fluid}}$ (Fig. 1H, dashed line).

4. Discussion

4.1. Comparison to Previous Studies

To consider the incorporation of Li in calcite, it is essential to examine the results from our precipitates alongside other comparable data from previous studies. Several experimental studies have investigated Li elemental and isotopic partitioning during inorganic precipitation of calcite (Okumura and Kitano, 1986; Marriott et al., 2004a, 2004b; Füger et al., 2019, 2022; Day et al., 2021; Seyedali et al., 2021). While these studies are all informative in the specific systems they explore, data from the majority cannot be directly compared to our data because of either fundamental differences in calcite precipitation approaches, substantial variability in solution chemistry during precipitation, or a lack of detailed reporting in experimental conditions. Day et al. (2021) conducted cave-analogue experiments, where calcite precipitation was driven by CO_2 degassing from a thin film of fluid which caused pH to increase by up to 0.8 units during precipitation. Seyedali

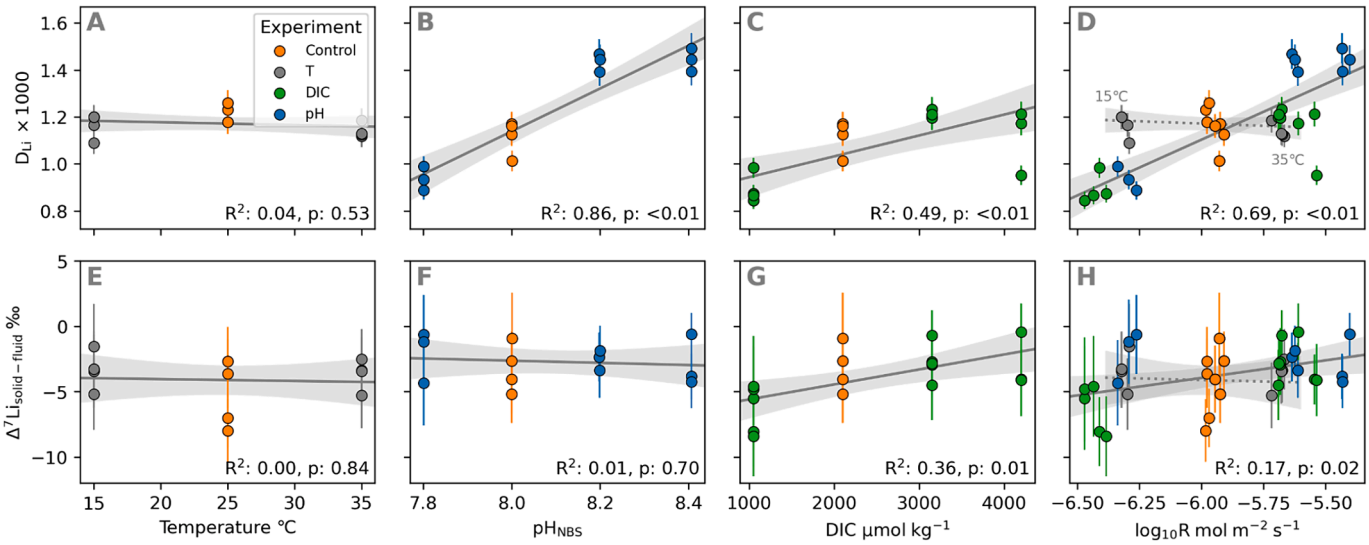

Fig. 1. Influence of individual precipitation conditions on D_{Li} and Δ^7Li. We find no significant relationship between D_{Li} and temperature (A), but significant positive correlations between D_{Li} and pH (B), DIC (C) and $log_{10}R$ (D). We find no correlations between Δ^7Li and temperature (E) or pH (F), but positive correlations with DIC (G) and $log_{10}R$ (H). Grey lines and shaded envelopes show linear best fits to the data with a 95% confidence interval; lines are intended as a visual aid to indicate the direction and significance of relationships, and should not be taken to imply a causal relationship. The p values indicating the significance of any correlations are calculated using a Wald test, which tests the null hypothesis that the slope of the data is zero. The dashed line and shaded envelope in (D) and (H) identify the trend of the temperature experiments only within the precipitation rate relationship, but statistics refer solely to the solid grey line fitting data from the pH and DIC experiments.

et al. (2021) precipitated calcite from vaterite precursors via phase transformation (i.e., dissolution-reprecipitation cycles), which induced pH changes up to 0.9 units in some of their experiments. In both these studies the pH variability within a single experiment is often larger than the entire pH range explored in our study, so it is not possible to compare our data to either study. Studies by Okumura and Kitano (1986) and Marriott et al. (2004a,2004b) do not report solution saturation state or area-normalised precipitation rates, which are necessary for useful comparison to our data. The temperature experiments of Marriott et al. (2004a) do, however, provide a useful reference point to provide context

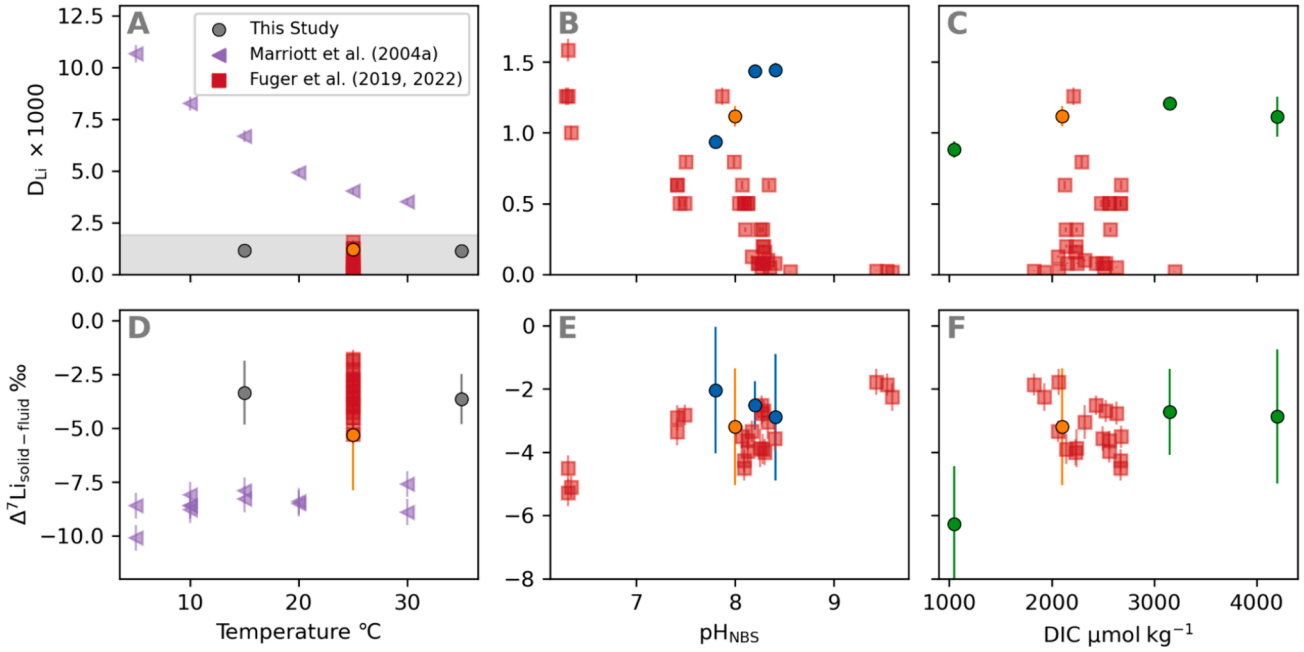

Fig. 2. Comparison of our data to previous inorganic precipitation studies measuring both D_{Li} and $\Delta^7Li_{solid\text{-}fluid}$. A previous study varying temperature (Marriott et al., 2004a) reports a strong negative relationship with D_{Li} (A) and weak positive relationship with $\Delta^7Li_{solid\text{-}fluid}$ (D), neither of which are present in our data. Previous studies of pH (B & E) and DIC (C & F) (Füger et al., 2019 & 2022) report a strong negative relationship between pH and D_{Li} (B) and weak positive correlation with $\Delta^7Li_{solid\text{-}fluid}$ (E). We observe an opposing trend in D_{Li}, and no significant effect in $\Delta^7Li_{solid\text{-}fluid}$ (Fig. 1 B & F). The same studies report no consistent patterns with DIC, whereas we observe positive correlations with both D_{Li} and $\Delta^7Li_{solid\text{-}fluid}$ (Fig. 1 C & G). For the Füger et al. data, D_{Li} data are from Füger et al. (2019) and $\Delta^7Li_{solid\text{-}fluid}$ data for a subset of the same samples are from Füger et al. (2022). Marriott et al. (2004a) report much higher D_{Li} than other experiments, so the y-axis for panel A is different from B & C, and D is different from E & F. The y-axis range of B & C is indicated by the horizontal grey bar in (A). Colours for data from This Study are the same as in Fig. 1. See Section 4.1 for our data selection criteria for the data comparisons shown here.

to our experiments. The two studies by Füger et al. (2019,2022) report full solution chemistry and precipitation rate data, allowing useful comparison to the results of our study.

At first consideration, there is little similarity between our data and those of previous comparable studies. The lack of relationship between temperature and D_{Li} (Fig. 1A) or $\Delta^7Li_{solid\text{-}fluid}$ (Fig. 1E) in our data are inconsistent with those of Marriott et al. (2004a), who reported a significant negative correlation between D_{Li} and temperature, and weak evidence for a slight positive trend in $\Delta^7Li_{solid\text{-}fluid}$ with temperature (Fig. 2 A & D). We further observed substantially lower average D_{Li} and higher $\Delta^7Li_{solid\text{-}fluid}$ values than Marriott et al. (2004a), indicating that there may be some fundamental unrecorded difference between the precipitation methods used in these studies.

The strong increase in overgrowth D_{Li} with solution pH in our data (Fig. 1B) is of similar slope but directly opposite to the negative relationship reported by Füger et al. (2019) (Fig. 2B). The lack of relationship between $\Delta^7Li_{solid\text{-}fluid}$ and pH is inconsistent with the positive relationship reported by Füger et al. (2022) in experiments spanning a much larger pH range (Fig. 2B; ~3 pH units, c.f. ~ 0.6 units in our study). The significant increase in D_{Li} with solution DIC (Fig. 1C) is consistent with the direction of the trend reported by Füger et al. (2019), but has a shallower slope in our data (Fig. 2C). The positive relationship between $\Delta^7Li_{solid\text{-}fluid}$ and DIC we observe (Fig. 1G) is inconsistent with the results of Füger et al. (2022), who report no significant trend with DIC (Fig. 2F) across a much narrower DIC range (~1000 μmol/kg c.f. 3000 μmol/kg).

While there is little overlap in the compositional trends with single solution variables, some coherent patterns do emerge when we consider Li incorporation as a function of precipitation rate (Fig. 3).

4.2. Precipitation rate effects on Li partitioning

Our data show that pH and DIC exert a strong influence on D_{Li} (Fig. 1A & B). However, when expressed as a function of precipitation rate (Fig. 1D), the data from these experiments fall on a single linear trend. This implies that the apparent effect of pH and DIC on D_{Li} is secondary, and that the variation in D_{Li} in these experiments is driven by kinetic processes associated with the change in precipitation rate, which in turn arises from variations in solution saturation state driven by modifying pH or DIC. Two different kinetic mechanisms might explain these patterns: the Surface Kinetic Model (SKM; DePaolo, 2011), or Growth Entrapment Model (GEM; Watson, 2004). These models invoke fundamentally different processes to explain changes in trace element partitioning and isotopic fractionation as a function of precipitation rate, and have each been applied to explain patterns trace element incorporation and isotopic fractionation in multiple geochemical systems. In the case of Li, Füger et al. (2019) suggest the GEM as a mechanism for the rate-dependence of D_{Li} observed in their data, but the same authors then invoke the SKM model to explain patterns in $\Delta^7Li_{solid\text{-}fluid}$ from precipitates grown in the same experiments (Füger et al., 2022). This illustrates that there is little consensus in the literature about which model should be used for specific geochemical systems or precipitation regimes. We do note, however, that it is highly unlikely that partitioning would be controlled by one mechanism, while isotopic fractionation is governed by the other in the same set of precipitates; the same mechanism should be invoked to explain patterns of partitioning and isotopic fractionation of a single trace element. For our purposes, it is sufficient to be aware that both mechanisms predict substantively similar geochemical patterns as a function of precipitation rate, and that we are unable to distinguish between them from the data in our experiments.

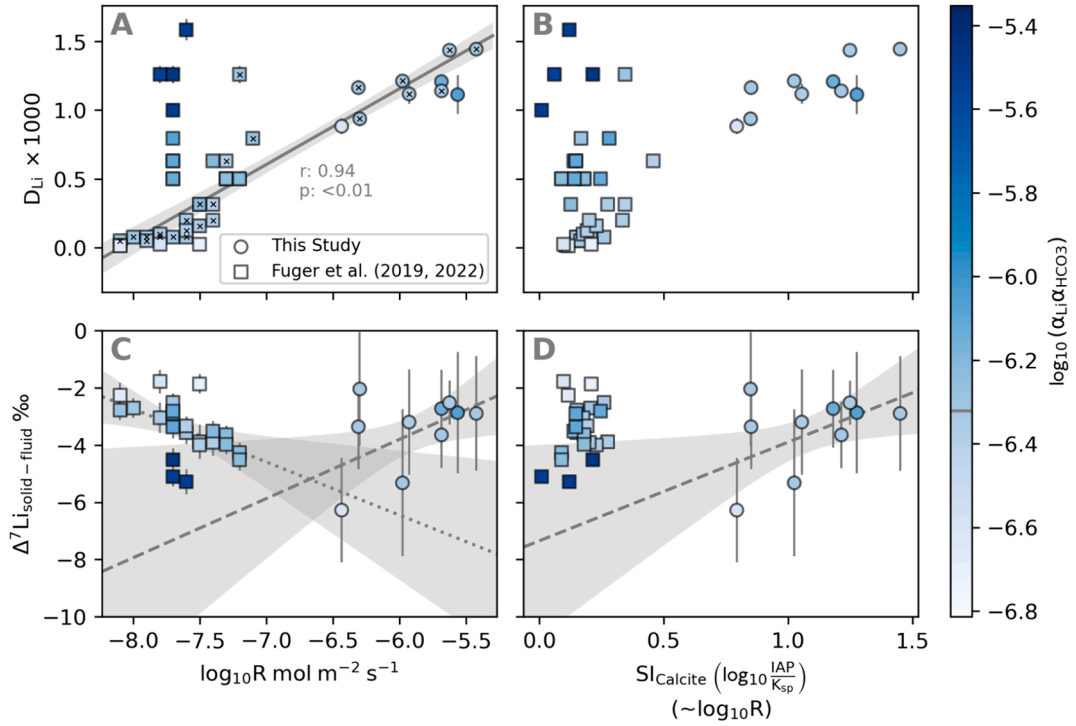

Fig. 3. The influence of precipitation rate and calcite saturation index on D_{Li} and $\Delta^7Li_{solid\text{-}fluid}$ in all paired data. Li partitioning data shows a dependence on both crystal precipitation rate (A) and solution saturation index (B), although the data deviate from this relationship as an approximate function of the $\{Li\}\{HCO_3^-\}$ ion activity product ($\alpha_{Li}\alpha_{HCO3}$) in the solution (higher partitioning at lower activities). At a constant $\alpha_{Li}\alpha_{HCO3}$ of $10^{-6.32 \pm 0.07}$ this precipitation rate relationship is well described by a linear fit (solid line and error envelope in A; points included in the fit are marked with an 'x'; displayed statistics are a Pearson R test). There is no consistent relationship between $\Delta^7Li_{solid\text{-}fluid}$ and calcite precipitation rate (C) or calcite saturation index (D), which are expected to be related by $R = k\,(S-1)^n$. In the data of Füger et al. (2019,2022) patterns in both D_{Li} and δ^7Li vary depending on whether they are considered relative to measured precipitation rates or calcite saturation index. Solid and dashed lines with error envelopes in C and D show linear trend lines and 95 % confidence intervals through our data (dashed) and the data of Füger et al (dotted), respectively, showing the inconsistent trends between these datasets.

Our data do not provide sufficient information to constrain a mechanistic model of the kinetic controls on D_{Li}.

Füger et al. (2019) observed an increase in D_{Li} with precipitation rate in experiments with much slower precipitation rates compared to our study. Our combined data therefore provide the opportunity to explore the processes of Li incorporation as a function of precipitation rate across a much larger range of conditions. Two simultaneous trends are apparent in the aggregate data: D_{Li} increases with both precipitation rate and the ion activity product of Li^+ and HCO_3^- ($a_{Li}a_{HCO3}$; Fig. 3A). At constant Li-HCO_3^- ion activity ($a_{Li}a_{HCO3} = 10^{-6.32 \pm 0.07}$) there is a significant (Pearson $r = 0.94$, $p < 0.01$) linear relationship between $\log_{10}R$ and D_{Li} across both datasets (Fig. 3A), which is likely attributable to purely kinetic processes. However, DePaolo's (2011) SKM model is unable to predict this trend with physically realistic parameters. Fitting this trend with the SKM model requires a backwards reaction rate (R_b; the rate at which Ca detaches from the surface of the crystal) ~ 3 orders of magnitude slower than has been determined for calcite (DePaolo, 2011). This parameter is considered to be a relatively invariant property of the mineral (DePaolo, 2011), so we conclude that the SKM model is unable to explain the patterns in our data. It is possible that the kinetic effect observed here is better described by the GEM model, but we have not attempted to fit the GEM model to our data because the code to conduct the relatively complex numerical simulations required by this model is not openly available, and a full re-implementation of this model is beyond the scope of this study. Despite this, we consider that a kinetic process is the most likely driver of these rate-dependent effects, as widely established in other trace element systems.

Within our combined data, D_{Li} deviates from the linear rate relationship as a function of the {Li}{HCO_3^-} ion activity product (indicated by $a_{Li}a_{HCO3}$ in Fig. 3), with higher D_{Li} values at higher activities, and vice versa. This implies that a primary kinetic control on D_{Li} is interacting with a secondary process that also modulates Li incorporation. We consider that this secondary process could be attributed to three possible mechanisms:

1. Some fraction of Li is incorporated from the solution as Li-HCO_3^0 ion pairs, as proposed by Füger et al. (2022). In this case, we would expect the deviation of D_{Li} from the rate trend to be positively correlated with the ion activity product $a_{Li}a_{HCO3}$.
2. Some fraction of Li is incorporated from the solution as Li-CO_3^- or Li_2-CO_3^0 ion pairs. In this case, we would expect the deviation of D_{Li} from the rate trend to be positively correlated with the ion activity product $a_{Li}a_{CO3}$.
3. Lithium in solution forms an association with free hydroxyl ions, creating Li-OH^0 pairs which must be broken before Li can be incorporated into the mineral. This would effectively reduce the activity of free Li in solution. In this case, we would expect the deviation of D_{Li} from the rate trend to be negatively correlated with the ion activity product $a_{Li}a_{OH}$.

We can explore these possibilities by considering the correlations between these solute ion activity products (IAP) and the residual between the data and the linear rate trend observed in the data (Fig. 4), assuming that the abundance of the ion pair in solution is directly related to the IAP in each case. There are significant correlations between each $\log_{10}$IAP and the offset from the linear precipitation rate trend. The correlation between the $\log_{10}(a_{Li}a_{CO3})$ is negative (Fig. 4A), which allows us to immediately disregard the possible role of Li-CO_3^- or Li_2-CO_3^0 as a means of elevating D_{Li} above the rate effect. However, we observe a positive trend in the residuals with $\log_{10}(a_{Li}a_{HCO3})$ and a negative trend with $\log_{10}(a_{Li}a_{OH})$, which could be consistent with either the incorporation of Li-HCO_3^0 ion pairs or a reduction in free Li^+ activity caused by the formation of Li-OH^0 ion pairs. Note that $\log_{10}(a_{Li}a_{HCO3})$ and $\log_{10}(a_{Li}a_{OH})$ are closely correlated in these data ($r = -0.81$, $p < 0.01$), so it is not possible to conclusively distinguish between these mechanisms. However, some insight may be gained by considering the relative magnitudes of the IAP in each case. Within these data, $a_{Li}a_{HCO3}$ ($10^{-6.7}$–$10^{-5.5}$) is 2–6 orders of magnitude higher than $a_{Li}a_{OH}$ (10^{-12}–10^{-8}). The variation in $a_{Li}a_{HCO3}$ is therefore much greater than $a_{Li}a_{OH}$, so may be more likely to modulate Li incorporation. This is consistent with the two-phase incorporation mechanism proposed by Füger et al. (2022), where both free Li^+ and Li-HCO_3^0 ion pairs are incorporated into calcite. However, additional work that explicitly separates $a_{Li}a_{HCO3}$ and $a_{Li}a_{OH}$ is required to conclusively test this.

A final line of reasoning that supports a role of Li ion pairing in modulating a kinetic control on Li incorporation comes from the effect (or lack thereof) of temperature on D_{Li}. Varying solution temperature drives changes in crystal precipitation rate via shifts in carbon speciation, calcite stability and precipitation kinetics. However, we see no significant variability in D_{Li} as a function of temperature (Fig. 1C). More importantly, D_{Li} in our temperature experiments does not follow the same rate relationship as the pH and DIC experiments (Fig. 1D). Overall, low-temperature precipitates had higher D_{Li} than predicted by the precipitation rate trend, whereas higher-temperature precipitates had lower D_{Li} than expected. This can also be interpreted as being consistent with the two-phase Li incorporation mechanism of Füger et al. (2022), if we consider the temperature dependence of the stability (and longevity)

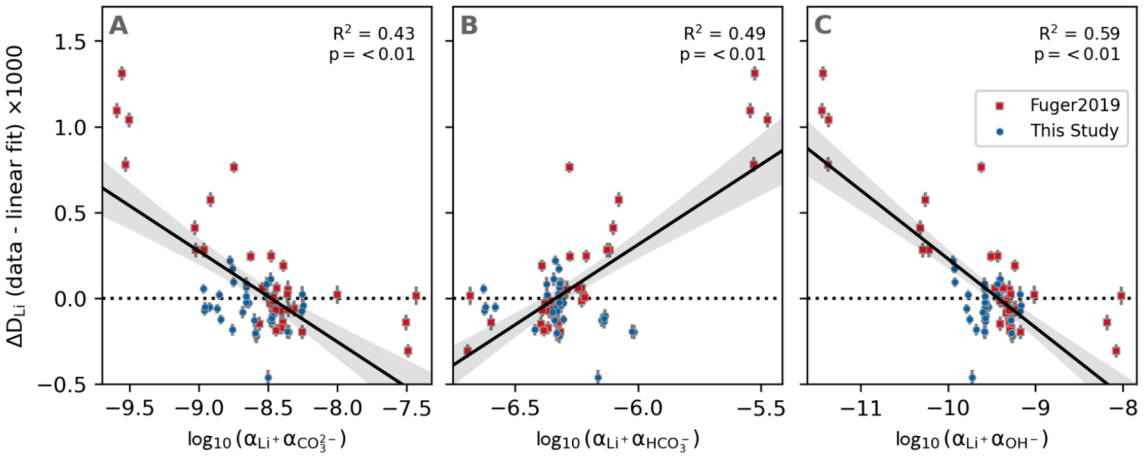

Fig. 4. The relationship between solution ion activity produces and linear fit residuals. The residual between the linear rate relationship (shown in Fig. 3A) and observed D_{Li} are plotted against the $\log_{10}$ of the IAPs $a_{Li}a_{CO3}$ (A), $a_{Li}a_{HCO3}$ (B), and $a_{Li}a_{OH}$ (C). The residual is significantly negatively correlated with $\log_{10}(a_{Li}a_{CO3})$ (A) and $a_{Li}a_{OH}$ (C), and significantly positively correlated with $\log_{10}(a_{Li}a_{HCO3})$ (B). Statistics on the plot show the R^2 values and p values of a Pearson test corresponding to the line of best fit shown on the plot.

of solute ion pairs. For example, measurements and modelling of water exchange rates in solutions (Hoffmann et al., 2012) indicate that the turnover of ion pairs in solution is faster at higher temperatures. From this, we would expect the Li-HCO_3^0 pair to be shorter-lived at high temperatures, and therefore less available for incorporation into a growing crystal. We note that this effect is relatively minor compared to the influence of precipitation rate, and that we therefore do not expect this to be a dominant control on Li partitioning in natural carbonates.

4.3. Controls on Li isotopic fractionation

Our $\Delta^7Li_{solid\text{-}fluid}$ data show no relationship with temperature or pH, and weak positive correlations with both DIC and precipitation rate (Fig. 1 D-F). This is distinct from D_{Li}, where positive correlations with both pH and DIC are underpinned by a strong positive correlation with precipitation rate. The lack of correlation between $\Delta^7Li_{solid\text{-}fluid}$ and pH implies a difference in the mechanisms underlying Li isotopic fractionation in each case, which is distinct from the kinetic controls on D_{Li}. This difference may arise from the distinct ways in which modifying DIC and pH alter solute chemistry. Increasing DIC at constant pH will raise both CO_3^{2-} and HCO_3^- in tandem, thus increasing both saturation and $\alpha_{Li}\alpha_{HCO3}$. Conversely, elevating pH at constant DIC increases CO_3^{2-} while decreasing HCO_3^-, thus increasing saturation while decreasing $\alpha_{Li}\alpha_{HCO3}$. In combination with the two-phase incorporation mechanism of Füger et al. (2022), we can hypothesise that two counteracting trends may combine to produce the observed patterns in $\Delta^7Li_{solid\text{-}fluid}$: a positive correlation with precipitation rate, and a positive correlation with $\alpha_{Li}\alpha_{HCO3}$. In the DIC experiments where precipitation rate and $\alpha_{Li}\alpha_{HCO3}$ increase together these trends combine to produce a positive relationship. Conversely, in the pH experiments where precipitation rate and $\alpha_{Li}\alpha_{HCO3}$ are anticorrelated, these trends cancel out to produce no variability in $\Delta^7Li_{solid\text{-}fluid}$. The positive correlation between $\Delta^7Li_{solid\text{-}fluid}$ and $\alpha_{Li}\alpha_{HCO3}$ would require that Li-HCO_3^0 ion pairs are incorporated into the crystal as a function of their abundance in solution, and are isotopically heavier than free Li^+ in solution.

No data or theoretical calculations are available on Li isotopic fractionation associated with the formation of Li ion pairs. However, the data of Füger et al. (2022), where precipitation rate and $\alpha_{Li}\alpha_{HCO3}$ vary independently, provide a means to test our hypothesis. Füger et al. (2022) report a ~ 3 ‰ decrease in $\Delta^7Li_{solid\text{-}fluid}$ with increasing precipitation rate at constant α_{HCO3}, and a ~ 4 ‰ decrease in $\Delta^7Li_{solid\text{-}fluid}$ with increasing $\alpha_{Li}\alpha_{HCO3}$ at constant precipitation rate (Fig. 3C). These patterns are inconsistent with both the positive precipitation rate trend observed in our data, and directly contradict our hypothesis that isotopically heavy Li-HCO_3^0 may drive a positive correlation between $\alpha_{Li}\alpha_{HCO3}$ and $\Delta^7Li_{solid\text{-}fluid}$. The separation of precipitation rate and $\alpha_{Li}\alpha_{HCO3}$ in the Füger et al. (2022) study provides a much better dataset to evaluate the impact of $\alpha_{Li}\alpha_{HCO3}$ on isotopic fractionation, and renders our hypothesised mechanism highly unlikely unless some difference in experimental setup might cause the isotopic fractionation associated with the formation of Li-X ion pairs to vary. There are two substantive differences in solution chemistry between the in our study and that of Füger et al. (2019,2022) that may give rise to differences in ion pairing behaviour: ionic strength (~0.025 in our study vs. ~ 0.3 in Füger et al.) saturation index (0.8–1.5 vs. 0–0.3). While we consider it unlikely that either of these differences would cause a reversal in the isotopic fractionation associated with forming Li-X ion pairs, we are unable to exclude the possibility that this is the case. We also note that the reversal of the relationship between $\Delta^7Li_{solid\text{-}fluid}$ and precipitation between our studies also provides strong evidence of some fundamental difference in either precipitation mechanism or solute chemistry.

We see no consistent pattern in $\Delta^7Li_{solid\text{-}fluid}$ between our data and that of Füger et al. (2022) (Fig. 3C). This is true both within each dataset, as Füger et al. (2022) report a negative correlation, while we find a positive correlation with precipitation rate (Fig. 1H), and in the aggregate data, where there is no clear correlation over the large precipitation rate range covered by both studies (Fig. 3C). Füger et al. (2022) proposed that the negative trend in their data may be explained by the Surface Kinetic Model mechanism (DePaolo, 2011), requiring a kinetic isotope fractionation of −8.8 ‰ $\Delta^7Li_{solid\text{-}fluid}$ at the faster precipitation rates examined in our study. Instead, we observe $\Delta^7Li_{solid\text{-}fluid}$ of −3.48 ± 0.56 ‰ (1σ, $n = 10$) at these precipitation rates. Alongside our finding that the SKM cannot predict patterns in D_{Li} with physically realistic parameters (see section 4.2), our new isotopic data suggest that the mechanism proposed by Füger et al. (2022) may not be universally applicable. Considered in aggregate, the most robust conclusion we can draw from the $\Delta^7Li_{solid\text{-}fluid}$ is that isotopic fractionation into calcite is constant with a mean value of −3.6 ± 2.8 ‰ (2σ, $n = 61$) across a wide range of precipitation rates, with no consistent pattern with any reported chemical or physical parameter.

4.4. Differences from Füger et al. (2019,2022)

The lack of a unifying patterns between our data and that of Füger et al. (2019,2022) may arise from differences in the methods used to estimate precipitation rate between the two sets of experiments (^{13}C mass balance in our study, Ca anomaly in Füger et al., 2019,2022). In seeded growth experiments, where classical crystal growth should dominate, we expect precipitation rate (R) to be a power-law function of solution saturation (S) as $R = k\,(S-1)^n$ (Morse et al., 2007), where $S = \{Ca^{2+}\}\{CO_3^{2-}\}/K_{sp}$. Close examination of the relationship between reported precipitation rates and solution saturation (Fig. S5) reveals a tight correlation between these parameters in our data, but a poor correlation in the data of Füger et al. (2019), who also conducted experiments at relatively low solution saturations. This either suggests that the uncertainty in the precipitation rate measurements of Füger et al. (2019) are large relative to the range in their experiments, or that there is some fundamental difference in crystal precipitation or Li incorporation mechanism between our two studies that leads to a decoupling between precipitation rate and saturation index in their experiments.

To determine whether this discrepancy may be obscuring coherent patterns between our two datasets, we additionally examine patterns in the data as a function of calcite saturation index ($SI_{calcite} = \log_{10}(S)$; Fig. 3B & 3D). We observe no substantive change in the patterns in our data as a function of log(R) or $SI_{calcite}$, but there are substantial changes in both D_{Li} (Fig. 3B) and $\Delta^7Li_{solid\text{-}fluid}$ (Fig. 3D) as a function of precipitation rate in the data of Füger et al. (2019,2022). Most significantly, when their data are plotted as a function of saturation index, the highest D_{Li} values are now those at the lowest saturation with the highest $\alpha_{Li}\alpha_{HCO3}$, and the trend between $\Delta^7Li_{solid\text{-}fluid}$ and precipitation rate is absent when considered as a function of $SI_{calcite}$. Note, however, that reconsidering the data of Füger et al. (2019,2022) as a function of $SI_{calcite}$ does not substantially alter our interpretation of our combined D_{Li} or $\Delta^7Li_{solid\text{-}fluid}$ data.

Unfortunately, the lack of agreement between these two datasets precludes the determination of a single mechanism that quantitatively explains Li incorporation and isotopic fractionation into calcite at this time, and more work is required to resolve this issue. Specifically, new experimental studies that span the entire range of calcite precipitation rates explored here and by Füger et al. (2019,2022) with a consistent experimental mechanism, while decoupling solution $\alpha_{Li}\alpha_{HCO3}$ and $\alpha_{Li}\alpha_{OH}$, and across a range of ionic strengths are strongly warranted. Robust parameterisation of the formation of Li ion pairs in solution would also prove invaluable, alongside first principles calculations of Li isotopic fractionation associated with the formation of these ion pairs.

4.5. Implications for the palaeo-proxy archive

Both the concentration (Li/Ca) and isotopic ratio (δ^7Li) of Li in foraminiferal calcite are utilised as paleoceanographic proxies for reconstruction of seawater carbonate chemistry (Vigier et al., 2015; Roberts et al., 2018), and to constrain the secular variations in seawater

δ^7Li (Misra & Froelich, 2012), respectively. The incorporation and isotopic fractionation of Li in biogenic calcite is determined by a combination of inorganic precipitation and biological mechanisms. While it is not possible to quantitatively transfer the results of our precipitation study to update our interpretation of palaeoclimate archives, our results are able to provide some insight into whether the geochemistry of Li in biogenic carbonates is primarily controlled by biological or inorganic processes.

We observe that partitioning of Li into inorganic calcite (D_{Li}) is independent of temperature but strongly dependent on mineral precipitation rate and $\alpha_{Li}\alpha_{HCO3}$, which gives rise to secondary trends with solution pH and DIC. This observation suggests that the relationship between Li/Ca and the seawater carbon system observed in biominerals (Lear et al.,2010; Lear & Rosenthal, 2015) may be driven by changes in the crystal precipitation rate of the biomineral. This does not preclude the presence of additional processes that might alter D_{Li}, such as modification of Li concentration at the site of calcification by biological ion transport mechanisms. Determination of in-situ precipitation rates of biominerals is required to identify whether D_{Li} in biominerals primarily depends on inorganic or biogenic factors. Despite these uncertainties, our results are consistent with foraminiferal Li/Ca being related to seawater carbonate chemistry via an inorganic process, increasing our confidence in its interpretation as a proxy archive for these parameters.

The lack of consistent pattern between $\Delta^7Li_{solid\text{-}fluid}$ and either crystal precipitation or any solution parameter observed in our study is encouraging for the use of natural calcites of abiogenic origins to generate a relatively robust record of solution δ^7Li (Pogge von Strandmann et al., 2017). However, our findings are unable to explain results from culture experiments showing that the δ^7Li of benthic foraminifera changes in response to seawater pH and/or [DIC] (Roberts et al., 2018; Vigier et al., 2015; Charrieau et al., 2023). This suggests that any variation observed in the δ^7Li of biomineral calcite is unlikely to be driven solely by inorganic precipitation processes, which then implies that δ^7Li in foraminiferal calcite is strongly sensitive to the biological processes of calcification (e.g. Li transport through Na^+/H^+ pumps; Busch et al., 1995). This raises the possibility that δ^7Li may be used as a tracer for seawater carbonate chemistry on a species-specific basis. However, this complicates the interpretation of δ^7Li as a faithful archive of seawater δ^7Li from biomineral carbonates (Misra and Froelich, 2012; Pogge von Strandmann et al., 2013) unless the carbonate chemistry sensitivity of each species is known and accounted for. Further work is needed to explore inter-species differences in the sensitivity of δ^7Li to seawater carbon chemistry to assess the potential significance of these effects.

5. Conclusions

We present D_{Li} and $\Delta^7Li_{solid\text{-}fluid}$ data from a series of inorganic calcite precipitation experiments where temperature, pH and DIC are independently varied. We identify strong positive correlations between D_{Li} and pH and DIC, but no relationship with temperature. We find no relationship between $\Delta^7Li_{solid\text{-}fluid}$ and either temperature or pH, but a weak positive correlation with DIC. Considered together, we confidently identify a strong precipitation rate control on D_{Li}, and find a weak positive relationship between $\Delta^7Li_{solid\text{-}fluid}$ and precipitation rate. Data from our temperature experiments go against this rate trend, implying that temperature exerts a secondary control on D_{Li} and $\Delta^7Li_{solid\text{-}fluid}$, causing it to deviate from the observed precipitation relationship.

When we consider our data alongside previous studies, we again find strong evidence for a precipitation rate control on D_{Li}, with a strong secondary control that is positively correlated with $\alpha_{Li}\alpha_{HCO3}$ and negatively correlated with $\alpha_{Li}\alpha_{OH}$. We consider that this is most likely attributable to the incorporation of Li-HCO_3^0 ion pairs, in agreement with the two-phase incorporation mechanism proposed by Füger et al. (2022). This is also consistent with the deviation from the precipitation rate trend with temperature, driven by the correlation between ion pair stability and temperature, where the incorporation of Li-HCO_3^0 ion pairs may be more favoured at lower temperatures. The story is less clear for $\Delta^7Li_{solid\text{-}fluid}$, where we observe no consistent relationships between our data and previously published data. The patterns reported in previous data are not reproducible in our experiments, and the most that can be said from the aggregate data is that $\Delta^7Li_{solid\text{-}fluid}$ is relatively stable across a wide range of conditions, with no clear consistent correlation with any reported experimental parameters. Additional work is required to ascertain the degree to which $\Delta^7Li_{solid\text{-}fluid}$ may be influenced by solution chemistry and precipitation conditions.

Data availability

Data are available through Zenodo at https://doi.org/10.5281/zenodo.11403415.

CRediT authorship contribution statement

Oscar Branson: Writing – review & editing, Writing – original draft, Visualization, Investigation, Formal analysis, Data curation, Conceptualization. **Joji Uchikawa:** Writing – review & editing, Writing – original draft, Methodology, Formal analysis, Data curation, Conceptualization. **Madeleine S Bohlin:** Writing – review & editing, Writing – original draft, Methodology, Formal analysis, Data curation. **Sambuddha Misra:** Writing – review & editing, Writing – original draft, Conceptualization.

Declaration of competing interest

The authors declare that they have no known competing financial interests or personal relationships that could have appeared to influence the work reported in this paper.

Acknowledgements

We would like to thank the Editor and Reviewers for their constructive comments on our manuscript. This research was supported by an Isaac Newton Trust Early Career Research Award and Leverhulme Trust Research Leadership Award (RL-2022-05) to OB, and US NSF Awards #1536743, #2001927, #2024631 and #2048436 to JU.

Appendix A. Supplementary material

A single file containing five supplementary figures, referred to in the text as Fig. S1-S5. Figures S1-S4 show titration records for precipitation experiments presented in the study. These plots show the amount of titrant added as a function of time to maintain the pH set-point in each experiment as the precipitate forms. Figure S5 shows a comparison between solution saturation state and reported precipitation rate in our data, and that of Füger et al. (2019,2022). Supplementary material to this article can be found online at https://doi.org/10.1016/j.gca.2024.07.001.

References

Beck, W.C., Grossman, E.L., Morse, J.W., 2005. Experimental studies of oxygen isotope fractionation in the carbonic acid system at 15°, 25° and 40°C. Geochim. Cosmochim. Acta 69, 3493–3503.

Bohlin, M.S., Misra, S., Lloyd, N., Elderfield, H., Bickle, M.J., 2018. High-precision determination of lithium and magnesium isotopes utilising single column separation and multi-collector inductively coupled plasma mass spectrometry. Rapid Commun. Mass Spectrom. 32, 93–104.

Busch, S., Burckhardt, B.-C., Siffert, W., 1995. Expression of the human sodium/proton exchanger NHE-1 in Xenopus laevis oocytes enhances sodium/proton exchange activity and establishes sodium/lithium countertransport. Pflugers Arch. 429, 859–869.

Carignan, J., Vigier, N., Millot, R., 2007. Three secondary reference materials for lithium isotope measurements: Li7-N, Li6-N and LiCl-N solutions. Geost and Geoanal Res. 31, 7–12.

Charrieau, L.M., Rollion-Bard, C., Terbrueggen, A., Wilson, D.J., Pogge von Strandmann, P.A.E., Misra, S., Bijma, J., 2023. Controls on lithium incorporation and isotopic fractionation in large benthic foraminifera. Minerals 13, 127.

Chen, D., Thibon, F., Felbacq, A., Weppe, L., Metian, M., Vigier, N., 2023. Coupled survey of lithium isotopes and Li/Ca in biogenic and inorganic carbonates. Earth Sci. Rev. 244, 104500.
Day, C.C., Pogge von Strandmann, P.A.E., Mason, A.J., 2021. Lithium isotopes and partition coefficients in inorganic carbonates: proxy calibration for weathering reconstruction. Geochim. Cosmochim. Acta 305, 243–262.
de Nooijer, L.J., Spero, H.J., Erez, J., Bijma, J., Reichart, G.J., 2014. Biomineralization in Perforate Foraminifera. Earth-Sci. Rev. 135, 48–58.
DePaolo, D.J., 2011. Surface kinetic model for isotopic and trace element fractionation during precipitation of calcite from aqueous solutions. Geochim. Cosmochim. Acta 75, 1039–1056.
Erez, J., 2003. The source of ions for biomineralization in foraminifera and their implications for paleoceanographic proxies. In: Dove, P., De Yoreo, J.J., Weiner, S. (Eds.), Biomineralization. Mineral. Soc. of Am, Washington, D.C., pp. 115–140
Füger, A., Konrad, F., Leis, A., Dietzel, M., Mavromatis, V., 2019. Effect of growth rate and pH on lithium incorporation in calcite. Geochim. Cosmochim. Acta 248, 14–24.
Füger, A., Kuessner, M., Rollion-Bard, C., Leis, A., Magna, T., Dietzel, M., Mavromatis, V., 2022. Effect of growth rate and pH on Li isotope fractionation during its incorporation in calcite. Geochim. Cosmochim. Acta 323, 276–290.
Hall, J.M., Chan, L.-H., McDonough, W.F., Turekian, K.K., 2005. Determination of the lithium isotopic composition of planktic foraminifera and its application as a paleo-seawater proxy. Mar. Geol. 217, 255–265.
Harris, C.R., Millman, K.J., van der Walt, S.J., et al., 2020. Array programming with NumPy. Nature 585, 357–362.
Hathorne, E.C., James, R.H., 2006. Temporal record of lithium in seawater: a tracer for silicate weathering? Earth Planet Sci. Lett. 246, 393–406.
Hoefs, J., Sywall, M., 1997. Lithium isotope composition of Quaternary and Tertiary biogenic carbonates and a global lithium isotope balance. Geochim. Cosmochim. Acta 61, 2679–2690.
Hoffman, A.E., Bourg, I.C., DePaolo, D.J., 2012. Ion desolvation as a mechanism for kinetic isotope fractionation in aqueous systems. Proc. Nat. Acad. Sci. USA 109, 18689–18694.
Hunter, J.D., 2007. A 2D graphics environment. Comput. Sci. Eng. 9, 90–95.
Lear, C.H., Rosenthal, Y., 2015. Benthic foraminiferal Li/Ca: Insights into Cenozoic seawater carbonate saturation state. Geology 34, 985–988.
Lear, C.H., Mawbey, E.M., Rosenthal, Y., 2010. Cenozoic benthic foraminiferal Mg/Ca and Li/Ca records: toward unlocking temperatures and saturation state. Paleoceanography 25, PA4215.
Lechler, M., Pogge von Strandmann, P.A.E., Jenkyns, H.C., Prosser, G., Parente, M., 2015. Lithium-isotope evidence for enhanced silicate weathering OAE 1a (Early Aptian Selli event). Earth Planet. Sci. Lett. 432, 210–222.
Marriott, C.S., Henderson, G.M., Belshaw, N.S., Tudhope, A.W., 2004a. Temperature dependence of δ^7Li, δ^{44}Ca and Li/Ca during growth of calcium carbonate. Earth Planet. Sci. Lett. 222, 615–624.
Marriott, C.S., Henderson, G.M., Crompton, R., Staubwasser, M., Shaw, S., 2004b. Effect of mineralogy, salinity, and temperature on Li/Ca and Li isotope composition of calcium carbonate. Chem. Geol. 212, 5–15.
Misra, S., Froelich, P.N., 2012. Lithium isotope history of Cenozoic seawater: changes in silicate weathering and reverse weathering. Science 335, 818–823.
Misra, S., Greaves, M., Owen, R., Kerr, J., Elmore, A.C., Elderfield, H., 2014. Determination of B/Ca of natural carbonates by HR-ICP-MS. Geochem. Geophys. Geosyst. 15, 1617–1628.
Morse, J.W., Arvidson, R.S., Lüttge, A., 2007. Calcium carbonate formation and dissolution. Chem. Rev. 107, 342–381.
Okumura, M., Kitano, Y., 1986. Coprecipitation of alkali metal ions with calcium carbonate. Geochim. Cosmochim. Acta 50, 49–58.
Parkhurst, D.L., Appelo, C.A.J., 1999. User's guide to PHREEQC (version 2) - a computer program for speciation, batch-reaction, one-dimensional transport, and inverse geochemical calculations. U.S. Geological Survey, Water-Resource Investigations Report 99-4259.
Pogge von Strandmann, P.A.E., Jenkyns, H.C., Woodfine, R.G., 2013. Lithium isotope evidence for enhanced weathering during Oceanic Anoxic Event 2. Nat. Geosci. 7.
Pogge von Strandmann, P.A.E., Vaks, A., Bar-Mattews, M., Ayalon, A., Jacob, E., Henderson, G.M., 2017. Lithium isotopes in speleothems: Temperature-controlled variation in silicate weathering during glacial cycles. Earth Planet. Sci. Lett. 469, 64–74.
Roberts, J., Kaczmarek, K., Langer, G., Skinner, L.C., Bijma, J., Bradbury, H., Turchyn, A. V., Lamy, F., Misra, S., 2018. Lithium isotopic composition of benthic foraminifera: a new proxy for paleo-pH reconstruction. Geochim. Cosmochim. Acta 236, 336–350.
Romanek, C.S., Grossman, E.L., Morse, J.W., 1992. Carbon isotope fractionation in synthetic aragonite and calcite: effects of temperature and precipitation rate. Geochim. Cosmochim. Acta 56, 419–430.
Sanyal, A., Nugent, M., Reeder, R.J., Bijma, J., 2000. Seawater pH control on the boron isotopic composition of calcite: evidence from inorganic calcite precipitation experiments. Geochim. Cosmochim. Acta 64, 1551–1555.
Seyedali, M., Coogan, L.A., Gillis, K.M., 2021. The effect of solution chemistry on elemental and isotopic fractionation of lithium during inorganic precipitation of calcite. Geochim. Cosmochim. Acta 311, 102–118.
The pandas development team, 2023. pandas-dev/pandas: Pandas (v2.0.3). Zenodo.
Uchikawa, J., Zeebe, R.E., 2012. The effect of carbonic anhydrase on the kinetics and equilibrium of the oxygen isotope exchange in the CO_2-H_2O system: Implications for δ^{18}O vital effects in biogenic carbonates. Geochim. Cosmochim. Acta 95, 15–34.
Uchikawa, J., Penman, D.E., Zachos, J.C., Zeebe, R.E., 2015. Experimental evidence for kinetic effects on B/Ca in synthetic calcite: Implications for potential $B(OH)_4^-$ and $B(OH)_3$ incorporation. Geochim. Cosmochim. Acta 150, 171–191.
Uchikawa, J., Harper, D.T., Penman, D.E., Zachos, J.C., Zeebe, R.E., 2017. Influence of solution chemistry on the boron content in inorganic calcite grown in artificial seawater. Geochim. Cosmochim. Acta 218, 291–307.
Uchikawa, J., Chen, S., Eiler, J.M., Adkins, J.F., Zeebe, R.E., 2021. Trajectory and timescale of oxygen and clumped isotope equilibration in the dissolved carbonate system under normal and enzymatically-catalyzed conditions at 25 °C. Geochim. Cosmochim. Acta 314, 313–333.
Uchikawa, J., Penman, D.E., Harper, D.T., Farmer, J.R., Zachos, J.C., Planavsky, N.J., Zeebe, R.E., 2023. Sulfate and phosphate oxyanions alter B/Ca and δ^{11}B in inorganic calcite at constant pH: crystallographic controls outweigh normal kinetic effects. Geochim. Cosmochim. Acta 343, 353–370.
Vigier, N., Rollion-Bard, C., Levenson, Y., Erez, J., 2015. Lithium isotopes in foraminifera shells as a novel proxy for the ocean dissolved inorganic carbon (DIC). Comptes Rendus Geosci. 347, 43–51.
Virtanen, P., Gommers, R., Oliphant, T.E., et al., 2020. SciPy 1.0: fundamental algorithms for scientific computing in Python. Nat. Methods 17, 261–272.
Watson, E.B., 2004. A conceptual model for near-surface kinetic controls on the trace-element and stable isotope composition of abiogenic calcite crystals. Geochim. Cosmochim. Acta 68, 1473–1488.
Zeebe, R.E., Wolf-Gladrow, D., 2001. CO_2 in seawater: Equilibrium, Kinetics, Isotopes. Elsevier Oceanography Series, 65. Elsevier, p. 346.
Zeebe, R.E., Sanyal, A., 2002. Comparison of two potential strategies of planktonic foraminifera for house building: Mg^{2+} or H^+ removal? Geochim. Cosmochim. Acta 66, 1159–1169.
Zhang, J., Quay, P.D., Wilbur, D.O., 1995. Carbon isotope fractionation during gas-water exchange and dissolution of CO_2. Geochim. Cosmochim. Acta 59, 107–114.